

Comparison between Computed Shearing Forces by AASHTO Specifications And Finite Element Method of Two Continuous Spans of Voided Slab Bridge

MAHER QAQISH¹, EMAD AKAWWI² AND EYAD FADDA^{3*}

¹Associate Professor, College of Engineering, Al-Balqa Applied University, Salt, Jordan

²Assistant professor at Al-Balqa Applied University-Salt-Jordan

³Assistant professor at Al-Balqa Applied University-Salt-Jordan

MAHER QAQISH
Al-Balqa Applied University
SALT- JORDAN
maherkakish@yahoo.com

abstract :- Voided slab bridge deck composed of two continuous span is 17.3m Long and 16m width with all over depth of 0.9m. The voided slab is composed of 20cm top and bottom slabs with circular voided areas of 50cm in diameter and center to center of these circles of 75cm. The locations of AASHTO loadings are positioned at certain points of deck slab to give maximum positive and negative shearings. These locations are determined from one dimensional model. The analysis of the bridge deck is carried out by two approaches. The first is AASHTO specifications where one dimensional approach is adopted and the second is three dimensional approach where finite element analysis is considered. The maximum shears obtained by both methods are found to be in good agreement with negligible differences.

Key-words: Bridges, voided slab, AASHTO Loadings and Finite Element Method.

* Corresponding author. E-mail: maherkakish@yahoo.com

1 Introduction

Bridges can be either concrete, timber and steel. Concrete bridges can be either cast insitu reinforced concrete or pre-stressed concrete or a combination of both. Reinforced concrete is well suited for use in bridges of all kinds due to its durability, rigidity and economy and aesthetic consideration [1].

The AASHTO specifications [2] specifies that diaphragms cast within the beam are recommended at midspan for spans up to 15.0m, at third points for spans is to 23m and at quarter points for spans over 23.0m.

Trejo [3] identifies the most significant parameters for evaluating the time to corrosion of reinforced concrete structures.

Suzuki [4] instrumented prestressed concrete (PC) box-girder bridge to monitor its surface and body temperature. The daily variations of temperature in the pavement and upper beam of the bridge were greater the deeper from the surface. During daytime on a fine day, bridge surface temperatures were higher than air temperatures, and at nighttime on a fine night, temperatures at the surface were lower than air temperatures. It is well known that sensible heat transfers depend on wind speed and surface temperature. The wind speed measured at the bridge and on the road revealed that the wind speed at the bridge was higher than at the road due to their topography. This wind effect during the daytime causes the surface temperature at the bridge to be lower than that at the road.

Thus, the reason why only bridge surfaces may freeze while roads do not can be explained by the fact that the surface temperatures of bridges are usually lower than those of roads, which can be attributed to their energy budget patterns caused by the wind speed differences between bridges and roads.

Potisuk [5] presented findings of field tests and analysis of two conventionally reinforced concrete (CRC) deck girder bridges designed in the 1950s. The bridges are in-service and exhibit diagonal cracks. Stirrup strains in the bridge girders at high shear regions were used to estimate distribution factors for shear. Impact factors based on the field tests are reported. Comparison of field measured responses with AASHTO factors was performed. Three-dimensional elastic finite-element analysis was employed to model the tested bridges and determine distribution factors specifically for shear.

Eight-node shell elements were used to model the decks, diaphragms, bent caps, and girders. Beam elements were used to model columns under the bent caps. The analytically predicted distribution factors were compared with the field test data. Finally, the bridge finite element modes were employed to compare load distribution factors for shear computed using procedures in the AASHTO LRFD and standard specifications.

Civjan [6] studied the use of integral abutment bridges for moderate spans throughout the United States. However, design methods and construction details vary from state to state. Variations between states are noted in the methods employed to accommodate deformations in the piles. The significance of these differences was evaluated through a finite-element study. The effects of backfill properties and soil restraint on piles were evaluated with regard to bridge distortions and maximum moment realized in the piles. Results show that bridge expansion is predominantly affected by backfill conditions, whereas contraction is influenced by pile restraint conditions.

Okui [7] presented a time-dependent finite-element analysis of a two I-girder composite bridge with a concrete slab. The creep and shrinkage of the concrete slab are considered as sources of time-dependent behavior. This analysis, unlike others, includes the shear – lag effect of the concrete slab on the time – dependent behavior of the two I-girder bridges.

Samaan [8] presented the results from a parametric study on the impact factors for 180 curved continuous composite multiple-box girder bridges. Expressions for the impact factors for tangential flexural stresses, deflection, shear forces and reactions are deduced for AASHTO truck loading. The finite-element method was utilized to model the bridges as three-dimensional structures.

The vehicle axle used in the analysis was simulated as a pair of concentrated forces moving along the concrete deck in a circumferential path with a constant speed. The effects of bridge configurations, loading positions, and vehicle speed on the impact factors were examined. Bridge configurations included span length, span-to-radius of curvature ratio, number of lanes, and number of boxes.

Najm [9] evaluated the behavior and performance of laminated circular elastomeric bearings and compares them to those of square and rectangular bearings. The experimental investigation studied the

bearings behavior in compression, compression and rotation, and compression and shear. Results from this limited study showed that the three bearings have similar stress-strain behavior in compression and they are in agreement with the AASHTO LRFD guide stress-strain curves.

In compression and rotation, the AASHTO LRFD substructure moments are slightly less than the measured values for circular bearings and rectangular bearings rotated about their strong axis for a compressive stress of 10.3 MPa (1.5 ksi) and slightly higher than those of rectangular bearings rotated about their weak axis. In compression and shear, the shear stiffness of circular and square bearings is in agreement with theoretical values within the range of design displacement.

Garrett [10] presented a case study that illustrated the effect of live dead loads, geometric nonlinear effects, temperature effects and material on load rating a two-span shallow concrete arch bridge. Presented are load ratings of the structure's arch ribs using a three-dimensional finite-element model with American Association of State Highway and Transportation Officials publications. As a result of this study, a refined analysis is recommended for load rating arch bridges.

Kayal [11] presented analytical methods to determine the plastic rotation capacity of reinforced cement concrete T-beam bridge girder (or grillage member) under the combined influence of flexure and torsion. The methods have been validated by experiments. The analytical methods are based on skew-bending and space truss theories. The tests have been carried out on 1:6 microconcrete models. The salient conclusions have been enumerated.

Trejo [12] provided a methodology by which design engineers can easily identify sensitive variables affecting the service life of RC structures exposed to potentially corrosive environments.

Guzda [13] developed a methodology incorporating real-time visual data collection from traffic cameras coupled with structural strain response of girder bridges. Average daily truck traffic along with frequency of multiple presences (same lane as well as adjacent lanes) and lane-wise truck traffic distribution were estimated for a steel-girder highway bridge on I-95 in Delaware. These data compared well with predictions from a Poisson process based model developed for this study.

Hon [14] presented a design method for assessing the restraint stiffness that exists for the slab of

typical beam-and-slab bridge decks and the strength enhancement due to compressive membrane action. This gives a more accurate prediction of the strength of the slab. The method has been developed through the laboratory testing of concrete specimens and the use of nonlinear finite element modeling.

Kirkpatrick [15] presented the results of tests carried out on a reinforced-concrete beam and slab bridge in Northern Ireland that incorporated novel reinforcement type and position. The research was aimed at extending previous laboratory tests on 1/3-scale bridge deck edge panels. The measured crack widths and deflections have been compared with the current code requirements.

Mankar [16] presented the prediction of the load distribution characteristics of straight composite multi-cell box girder bridges. A finite element analytical model based on the commercially available "ANSYS" software, has been used for the analyses. The analytical model is substantiated by published results from tests on composite concrete deck-steel three-cell bridge model.

A parametric study, using the finite element modeling, was conducted in which composite multi-cell bridge prototypes were analyzed to evaluate their load distribution factors for shear under IRC live loading condition. The key parameters considered in this study are: number and stiffness of cross-bracing and top-chord system, number of cells, number of lanes, and loading conditions.

Based on the parametric study, load distribution factors for shear is deduced. Recommendations to enhance the torsional resistance to static forces on this type of bridges are made. A recommendation for optimum spacing of cross bracings has been suggested. The results from this practical-design-oriented study would assist the bridge engineer to design composite cellular bridges more reliably and economically.

Dwivedi [17] presented a finite element analysis to predict the nonlinear temperature distributions and their response for the design of concrete bridges, which takes into consideration the various meteorological, environmental, and other bridge parameters. The proposed model has been validated against the results obtained by an experimental program on a laboratory model of concrete box-girder bridge exposed to solar radiation. The proposed analytical model has been validated against the experimentally observed values on laboratory models of concrete box girder bridge.

Good agreement has been observed between the computed and experimental thermal profiles.

Manassa [18] the effect of a skew angle on simple-span reinforced concrete bridges using the finite-element method. The parameters investigated in this analytical study were the span length, slab width, and skew angle. The finite-element analysis (FEA) results for skewed bridges were compared to the reference straight bridges as well as the American Association for State Highway and Transportation Officials (AASHTO) Standard Specifications and LRFD procedures. A total of 96 case study bridges were analyzed and subjected to AASHTO HS-20 design trucks positioned close to one edge on each bridge to produce maximum bending in the slab.

The AASHTO Standard Specifications procedure gave similar results to the FEA maximum longitudinal bending moment for a skew angle less than or equal to 20° . As the skew angle increased, AASHTO Standard Specifications overestimated the maximum moment by 20% for 30° , 50% for 40° , and 100% for 50° .

The AASHTO LRFD Design Specifications procedure overestimated the FEA maximum longitudinal bending moment. This overestimate increased with the increase in the skew angle, and decreased when the number of lanes increased; AASHTO LRFD overestimated the longitudinal bending moment by up to 40% for skew angles less than 30° and reaching 50% for 50° . The ratio between the three-dimensional FEA longitudinal moments for skewed and straight bridges was almost one for bridges with skew angle less than 20° . This ratio decreased to 0.75 for bridges with skew angles between 30° and 40° , and further decreased to 0.5 as the skew angle of the bridge increased to 50° .

This decrease in the longitudinal moment ratio is offset by an increase of up to 75% in the maximum transverse moment ratio as the skew angle increases from 0 to 50° . The ratio between the FEA maximum live-load deflection for skewed bridges and straight bridges decreases in a pattern consistent with that of the longitudinal moment. This ratio decreased from one for skew angles less than 10° to 0.6 for skew angles between 40° and 50° .

Yehia [19] studied the different nondestructive evaluation techniques used in the assessment of concrete bridge deck conditions. An experimental investigation to evaluate the ability of infrared thermography, impact echo, and ground penetrating

radar to detect common flaws in concrete bridge decks is developed and discussed.

Results from this study showed the ability of these methods to detect defects with varying precision. Capabilities of the methods were verified and comparisons among the methods were made.

Leem [20] performed Laboratory experiments on full-size girder specimens to evaluate possible deterioration in shear capacity under repeated loading. Specimen variables included: T and inverted-T configurations, stirrup spacing, and flexural reinforcing details. Test results indicated bond deterioration increased diagonal crack displacements, and analysis methods to predict the shear capacity of diagonally cracked reinforced concrete girders subjected to high-cycle fatigue damage are provided. The AASHTO-LRFD shear provides conservatively predicted shear capacity for the fatigued specimens without stirrup fractures, and shear capacity predictions from computer analysis program response 2000 were very well correlated with experimental result for fatigued test specimens when the input concrete tensile strength was reduced to nearly zero.

Samman [21] studied continuous curved composite multiple-box girder bridges, using the finite-element method, to evaluate their natural frequencies and mode shapes. Experimental tests are conducted on two continuous twin-box girder bridge models of different curvatures to verify and substantiate the finite-element model. Empirical expressions are deduced from these results to evaluate the fundamental frequency for such bridges.

The parameters considered herein are the span length, number of lanes, number of boxes, span-to-radius of curvature ratio, span-to-depth ratio, end-diaphragm thickness, number of cross bracings, and number of spans.

Zhang [22] conducted a theoretical study on the determination of the allowable differential settlement. The maximum transient vibration value of the acceleration is recommended as the vibration comfort index. A dynamic response analysis to Man-Vehicle-Road system is carried out by means of the Laplace transform in which the vehicle is modeled as a three-degree-of-freedom system, and the bridge approaches with and without approach-relative slopes are simplified as broken lines model and step model, respectively. Parametric studies are carried out to find out what kind of effects some parameters such as the driving direction and running

speed may have on the allowable differential settlement.

Finally, the method and computational procedures to determine the allowable differential settlement are presented.

2 Live Loads

The live loads of the AASHTO specifications [2] consist of standards trucks or of lane loads which consist of a uniformly distributed load and a concentrated load. The maximum truck loading is HS20 and it is designed by the indication HS20-44. This loading consists of a 3-axle vehicle with a total weight of 32.5 tons. Axle loads and dimensions of HS20-44 vehicle are shown in Fig.1. The lane loading as shown in Fig.2 is composed of distributed load plus concentrated loads.

The concentrated loads are composed of one load for bending and the other for shear as shown in Fig.2 These concentrated loads are located in certain positions, in addition to the distributed loads to give the maximum shear stresses.

Live load stresses due to truck loading (or equivalent lane loading) are increased to allow for vibration and the sudden application of the load. The increase is computed by the formula:

$$I = \frac{15.24}{L + 38} < 0.3 \quad (1)$$

Where:

I = the impact fraction of live load stress.

L = the loaded length in meters.

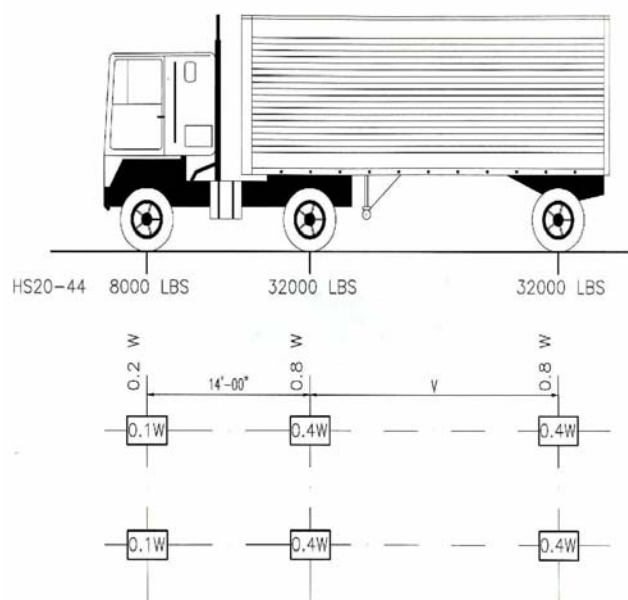
To encounter the unexpected traffic loadings, these loadings are multiplied by 1.5. Study of axle weight in Jordan is illustrated in 56, 57.

Standard truck or lane loading is assumed to occupy a loaded width of 10ft (3.048m). These loads shall be placed in 12ft (3.65m) wide design traffic lanes spaced across the entire bridge roadway width in number and position required to produce the maximum stress in the member under consideration. The uniform and concentrated load of a lane loading shall be considered to be uniformly distributed over a 10ft (3.048m) width on a line normal to the centerline of the lane. In computing stresses, each 10ft lane loading or single standard truck shall be considered as a unit that can occupy position within its individual traffic lane, so as to produce maximum stress. Fractional load lane widths or fractional trucks shall not be used.

For continuous spans, only one standard **H** or **HS** truck per lane shall be considered and placed so as

to produce maximum positive or negative moments. The type of loading used, whether lane loading or truck loading and whether the spans are simple or continuous, shall be the loading which produces the maximum stress. Where maximum stresses are produced in any member by loading any member of traffic lanes simultaneously, the following percentage of the resultant live load stress shall be in view of improbable coincident maximum loading:

- 100% One or two lanes
- 90% Three lanes
- 75% Four lanes or more



W = Combined weight on the first two axles which is the same as for the corresponding H truck.

V = Variable spacing – 14 feet to 30 feet inclusive. Spacing to be used is that which produces maximum stress.

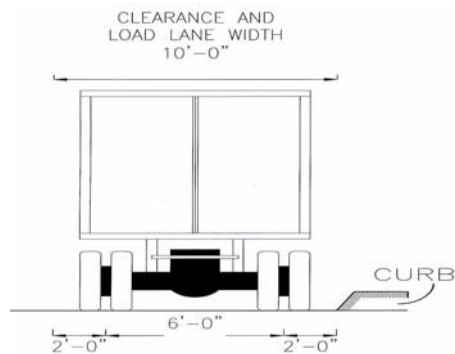


Fig.1 AASHTO TRUCK LOADING HS 20-44

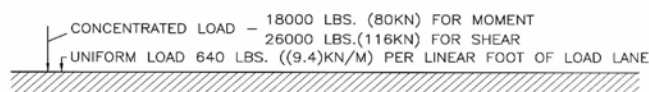


Fig.2 LANE LOADING HS 20-44

3 Distribution Of Live Loads:

When a concentrated load is placed on a bridge deck, the load is distributed over an area larger than the actual contact area. Hence, a larger portion of the deck will assist in resisting the load. This is described as load distribution and has been taken into account in AASHTO specification [2].

According to AASHTO specification [2], no longitudinal distribution of the wheel loads shall be assumed in calculating bending moments in longitudinal beams. The lateral distribution shall be determined as follows:

1. The distribution of wheel loads for each interior longitudinal beam of a reinforced concrete box girder bridge designed for two or more traffic lanes should be taken as $S/2.134$, where S is the spacing of longitudinal beams in meters.
2. The distribution of wheel loads for exterior roadway beams of a reinforced concrete box girder bridge should be taken as $We/2.134$. The width (We) to be used in determining the wheel line distribution to the exterior girder is the top slab width as measured from the midpoint between girders to the outside edge of the slab. In no case shall exterior beam have less carrying capacity than an interior beam.

The common methods used in bridge design is either grillage or finite element or **AASHTO**.

4 Grillage Analysis :

This methods is usually used for analysis of bridges were based on the consideration of the bridge deck as an elastic continuum in the form of an orthogonally anisotropic plate. Using the stiffness method of structural analysis, it became possible to analyze the bridge deck structure as an assembly of elastic structural members connected together at discrete nodes. There are four distinct techniques which have been found useful be bridge engineers: grillage and space frame analysis, folded plate method, finite element method and finite strip method.

The grillage analogy method bridge involves a plane grillage of discrete interconnected beams.

The grillage analogy has become popular because of the following reasons:

- It can be used in cases where the bridges exhibits complicating features such as a heavy skew, edge stiffening and deep hunches over supports.
- The representation of a bridge as a grillage is ideally suited to carrying out the necessary calculations associated with analysis and design on a digital computer.
- The grillage representation is conducive to giving the designer an idea bout the structure behavior of the bridge and the manner in which bridge loading is distributed and eventually taken to the supports [23].

It is a horizontal grid consisting of the main (longitudinal) and cross (transverse) girders are orthogonally intersecting and is subjected to vertical loads only. Each of the longitudinal girders having flexural stiffness (EI), torsional stiffness (GJ) and length (L). The longitudinals girder are spaced a distance (h) apart and are interconnected by a number of equally spaced transverse beams each of which has flexural stiffness (EI_T) and torisonal stiffness (GJ_T) [23].

In a grillage analysis, the elements of a grid are assumed to be rigidly connected, so that the original angles between elements connected together at a node remain unchanged. Both torisonal and bending moment continuity then exist at the node point of a grid [24]. Each beam element is assumed to have three degree of freedom at each end. These consist of two rotations and a transverse displacement as shown in Figure.3.

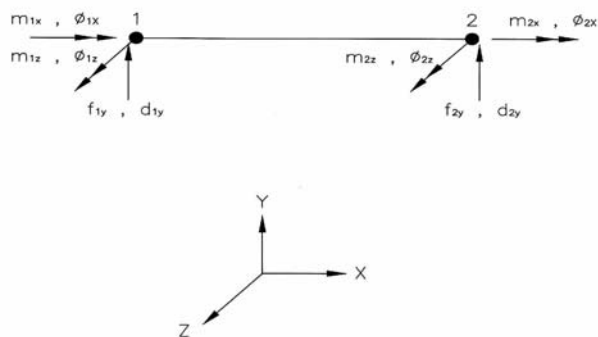


Fig.3 GRID ELEMENT WITH NODAL DEGREES OF FREEDOM AND NODAL FORCES.

Using the direct stiffness method, we can obtain the stiffness matrix for an orthogonal grillage members from the following equations:

$$\{F\} = [K] * [\Delta] \quad (2)$$

In matrix form as follows:

$$\begin{bmatrix} f_{1y} \\ m_{1x} \\ m_{1z} \\ f_{2y} \\ m_{2x} \\ m_{2z} \end{bmatrix} \begin{bmatrix} \frac{12EI}{L^3} & 0 & \frac{6GEI}{L^2} & \frac{-12EI}{L^3} & 0 & \frac{6EI}{L^2} \\ 0 & \frac{GJ}{L} & 0 & 0 & \frac{-GJ}{L} & 0 \\ \frac{6EI}{L^3} & 0 & \frac{4EI}{L} & \frac{-6EI}{L^3} & 0 & \frac{2EI}{L} \\ \frac{-12EI}{L^3} & 0 & \frac{-6EI}{L^2} & \frac{12EI}{L^3} & 0 & \frac{-6EI}{L^2} \\ 0 & \frac{-GJ}{L} & 0 & 0 & \frac{GJ}{L} & 0 \\ \frac{6EI}{L^3} & 0 & \frac{2EI}{L} & \frac{-6EI}{L^3} & 0 & \frac{4EI}{L} \end{bmatrix} \begin{bmatrix} d_{1y} \\ \phi_{1x} \\ \phi_{1z} \\ d_{2y} \\ \phi_{2x} \\ \phi_{2z} \end{bmatrix}$$

Where:

The global stiffness matrix KG for members which do not intersect at right angles can be found from the following equation:

$$[K_G] = [\lambda_G]^T * [K] * [\lambda_G] \quad (3)$$

Where:

[K]: element stiffness matrix.

[\lambdaG]: 6 by 6 transformation matrix.

The transformation matrix relating local to global degree of freedom is given by:

$$[\lambda_G] = \begin{bmatrix} 1 & 0 & 0 & 0 & 0 & 0 \\ 0 & C & S & 0 & 0 & 0 \\ 0 & -S & C & 0 & 0 & 0 \\ 0 & 0 & 0 & 1 & 0 & 0 \\ 0 & 0 & 0 & 0 & C & S \\ 0 & 0 & 0 & 0 & -S & C \end{bmatrix}$$

Where:

$$C = \cos\theta = \frac{X_1 - X_2}{L}, S = \sin\theta = \frac{Z_1 - Z_2}{L} \quad (4)$$

Where L is length of the element from node i to node j.

5 Idealization of Deck:

As a first step in a grillage analysis, the continuum of the deck must be idealized into a series of a discrete members. The idealization was performed using the following guidelines:

- f_{1y} : shear force in y-axis at node 1.
- m_{1x} : torsion moment about x-axis at node 1.
- m_{1z} : bending moment about z-axis at node 1.
- f_{2y} : shear force in y-axis at node 2.
- m_{2x} : torsion moment about x-axis at node 2.
- m_{2z} : bending moment about z-axis at node 2.
- d_{1y} : displacement in y-axis at node 1.
- φ_{1x} : torsion rotation about z-axis at node 1.
- φ_{1z} : bending rotation about z-axis at node 1.
- d_{2y} : displacement in y-axis at node 2.
- φ_{2x} : torsion rotation about x-axis at node 2.
- φ_{2z} : bending rotation about z-axis at node 2.

Table 1: Torsional coefficient (K) for rectangular sections

a b	1	1.2	1.5	1.75	2.0	2.25
K	0.141	0.166	0.196	0.213	0.229	0.24
a b	2.5	3.0	4.0	5.0		
K	0.249	0.263	0.281	0.291		

1. The logical choice of longitudinal grillage beams is to have them coincident with the physical (actual) beams. The centre lines of the grillage beams are coincident with the center lines of the physical beam, as a general rule, one grillage beam does not replace more than two physical beams. When dealing with member properties, the members are given the properties of the girders plus associated portions of the slab, according to the following equations [23].

$$I_x = I_{\text{comp}} \quad (5)$$

$$J_x = J_g + \frac{L_y t^3}{6} \quad (6)$$

Where:

I_x : second moment of area of the longitudinal members.

I_{comp} : second moment of area of the composite girder and slab section.

J_x :torsional inertia of the longitudinal members.

J_g : torsional inertia of the girder section.

L_y : spacing of the longitudinal members.

t : thickness of the deck slab.

2. The torsional inertias for an I or T-sections can be calculated using the following equation:

$$J = Kab \quad (7)$$

Where a is greater than b and K coefficient can be obtained from Table 1.

3. The transverse deck slab is consist of a number of transverse strips, and each strip is replaced by a beam. In which case their properties are calculated in the same way as for slab bridge [23]. Thus:

$$I_z = \frac{L_x t^3}{12} \quad (8)$$

$$J_z = \frac{E_c L_x t^3}{G_c 12} \quad (9)$$

Where:

I_z : second moment of area of the transverse members.

J_z : torisonal inertia of the transverse members.

L_x : spacing of the transverse members.

E_c : modulus of elasticity of the deck slab material.

G_c : shear modulus of the deck slab material.

It is not usually obvious how to define the positions of the transverse grillage beam except in the case where diaphragms exist within the span, in which case the idealized beams should be in the same positions as the physical beams. For decks with only top slab in the transverse direction, suggested that transverse grillage beams are substituted at [23].

- a. The abutments (where in most cases there will be diaphragm).
- b. Intermediately such that the ratio of spacing of transverse grillage beams to the spacing of longitudinal grillage beams is approximately 1.5:1.
- c. The total number of transversals is odd and not less than five. Two important points should be emphasized regarding:
 1. All calculations are based on gross-sections, neglecting reinforcement and cracking of the concrete.
 2. Poisson's ratio effects where neglected because they are limited to the deck slab.

6 Finite Element Method:

The finite element method is a well known tool for the solution of complicated structural engineering problems, as it is capable of accommodating many complexities in the solution. In this method, the actual continuum is replaced by an equivalent idealized structure composed of discrete elements, referred to as finite elements, connected together at a number of nodes.

The finite element method was first applied to problems of plane stress, using triangular and rectangular element. The method has since been extended and we can now use triangular and rectangular elements in plate bending, tetrahedron and hexahedron in three-dimensional stress analysis, and curved elements in singly or doubly curved shell problems. Thus the finite element method may be seen to be very general in application and it is

sometimes the only valid form of analysis for difficult deck problems.

The finite element method is a numerical method with powerful technique for solution of complicated structural engineering problems. It most accurately predicted the bridge behavior under the truck axle loading [26].

The finite element method involves subdividing the actual structure into a suitable number of sub-regions that are called finite elements. These elements can be in the form of line elements, two dimensional elements and three dimensional elements to represent the structure.

The intersection between the elements are called nodal points in one dimensional problems where in two and three dimensional problems are called nodal lines and nodal planes respectively. At the nodes, degrees of freedom (which are usually in the form of the nodal displacement and/ or their derivatives, stresses, or combinations of these) are assigned. Models which use displacements are called displacement models and some models use stresses defined at the nodal points as unknown. Models based on stresses are called force or equilibrium models, while those based on combinations of both displacements and stresses are termed mixed models or hybrid models [24].

Displacements are the most commonly used nodal variables, with most general purpose programs limiting their nodal degree of freedom to just displacements. A number of displacement functions such as polynomials and trigonometric series can be assumed, especially polynomials because of the ease and simplification they provide in the finite element formulation.

To develop the element matrix, it is much easier to apply a work or energy method. The principle of virtual work, the principle of minimum potential energy and castigliano's theorem are methods frequently used for the purpose of derivation of element equation.

The finite element method has a number of advantages, they include the ability to [25]:

- Model irregularly shaped bodies and composed of several different materials.
- Handle general load condition and unlimited numbers and kinds of boundary conditions.
- Include dynamic effects.
- Handle nonlinear behavior existing with large deformation and non-linear materials.

7 Idealization of Structure:

A mathematical model of the structure is formulated in which it is represented as an assemblage of discrete elements. Each element has its own shape, thickness, material properties and even external load effects.

These elements can be in the form of line elements, two dimensional plane stress or plane strain elements, flexural, plate, and/or shell elements, axisymmetric elements, general three dimensional solid elements. Figure.4 show some frequently used elements [26].

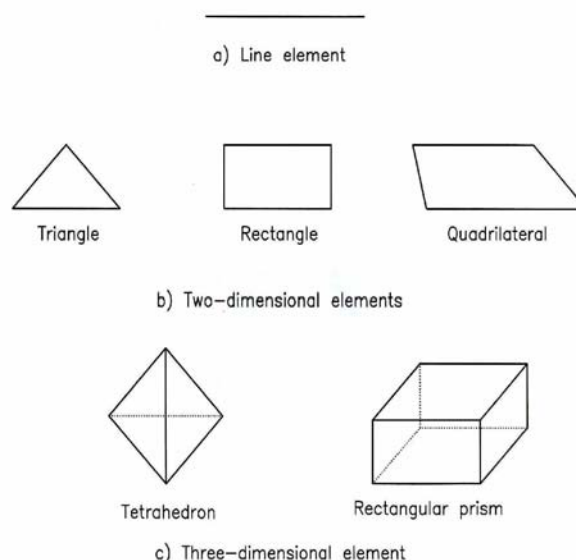


Fig.4 ELEMENT MODELS.

The model of elements depends on the geometry of the structure, the local features such as stress concentration and the convergence properties of the element. For slab deck, the element model may be taken as a triangular or quadrilateral plate element.

8 Generation of Element Stiffness Matrix :

For an element, a stiffness matrix K is a matrix such that $f = kd$, where k relates local coordinate (x, y, z) nodal displacements d to local forces f of a single element.

The stiffness matrix k and the local forces matrix f are evaluated based on the virtual work principle according to the following equation:

$$K = \int B^T E B dv \quad (10)$$

$$F = \int_s N^T T ds + \int_v N^T X dv + N^T P \quad (11)$$

Where:

To obtain the global stiffness matrix for the whole structure, the element stiffness matrix K for each element can be added together using a method of superposition called the direct stiffness method whose basis is nodal force equilibrium. Implicit in the direct stiffness method is the concept of continuity, or compatibility, which requires that the structure remain together and that no tears or overlaps occur anywhere in the structure.

The global stiffness matrix is singular, that is, its determinate vanishes, and there can be an infinite number of possible solutions. To remove this singularity, it must invoke certain boundary conditions. When introducing the boundary conditions, the displacement or stresses usually are called primary unknowns or primary quantities can be found at all nodes of the structure. With these unknowns established, the quantities such as strains, shear forces can be evaluated.

9 Analysis of Finite Element Using STADD III:

As excellent summary of the scope of finite element using **STADD III** [27] can be done by taking into consideration the following three basic phases:

9.1 Theoretical Basis:

The principle of the **STADD III** [27] plate finite element is based on hybrid finite element formulations. The distinguishing features of this finite element are as follows:

- These elements are available as triangles and quadrilaterals, with corner nodes only, with each node having six degree of freedom.
- These elements may be connected to plan or

B : ∂N , where N : shape function matrix.

E : modulus of elasticity matrix.

T : surface force matrix.

X : body force matrix.

P : nodal load matrix.
space frames.

9.2 Geometry Modeling:

When the **STADD III** [27] generating the finite

element, the following points should be considered:

- The program automatically generates a fifth node (center node) at the element center.
- Element nodes should be specified either clock wise or counter clock wise.
- The precise orientation of local coordinates is determined as follows:
 - a. Designate the mid points of the four elements edges IJ, JK, KL, LI by M, N, O, P respectively.
 - b. The vector pointing from p to N is defined to be the local x -axis.
 - c. The cross product of vectors PN and MO defines the local z -axis,
 1. i. e., $Z = PN \times MO$
 - d. The cross product of vectors Z and X defines the local Y -axis,
 1. i.e. $Y = Z \times X$

Figure.5 shows the local coordinates orientation.

- Element aspect ratio should be on the order 1:1, and preferably less than 4:1.
- The angles between two adjacent element sides should not be much larger than 90° and never larger than 180° .

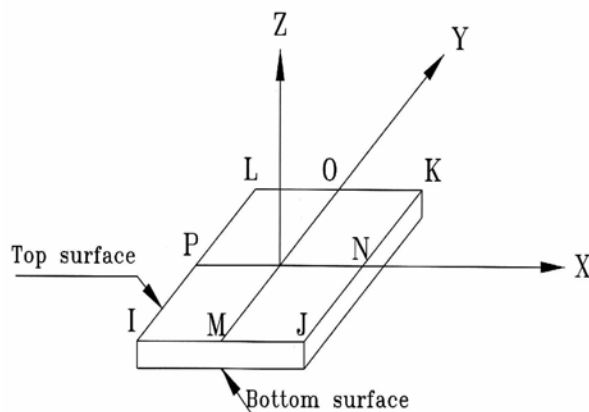


Fig.5 ELEMENT LOCAL AXIS SYSTEM.

10 Structural Idealization

The bridge is composed of 2 continuous spans each 17.3m with 20cm top and bottom slabs and 50cm the height of the web. Plane of the bridge is shown in Fig.6 Transverse section is shown in Fig.7. Longitudinal section is shown in Fig.8. The width of top slab is 16m and the width of bottom slab is 15.0m. One Fixed electrometric bearing pad support at the middle pier and two guided electrometric bearing pads supports at the abutment are provided.

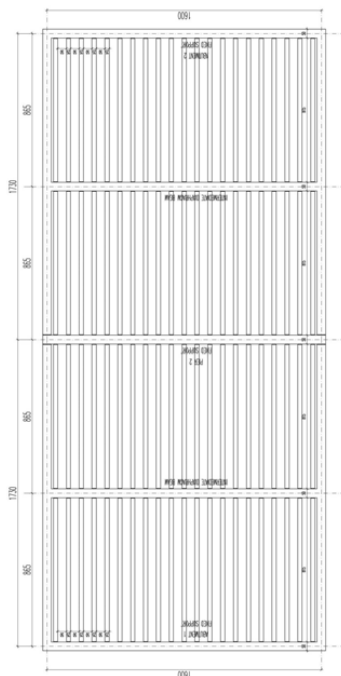


Fig. 7 TRANSVERSE SECTION OF VOIDED SLAB.



Fig. 8 LONGITUDINAL SECTION OF VOIDED SLAB.

The bridge is analyzed as one dimensional structure. Each span is divided to 10 points and at each point the shearing forces are calculated based on influence lines.

The shearing forces are calculated due to dead and live loads. The dead loads composed of the own weight of the concrete box and the wearing surface.

The live load is according to **AASHTO** specification. HS 20-44 and Lane Loading are considered in the analysis and the one which gives higher shear is taken into consideration.

Then a three dimensional finite element model of the bridge is considered. The top and the bottom slabs are divided to a horizontal finite element mesh, while the webs are divided to vertical finite element mesh. The **AASHTO** live loads are applied at the top mesh at certain points located especially for that purpose.

The locations of these truck loadings are determined from the first model. The asphalt layer is considered as a pressure load on the finite element mesh. The dead weight of the superstructure is considered in this model.

Combinations of all the above mentioned loads are considered in this analysis. The live loads are located in a certain positions to give maximum shearing force. Fig .9 shows the finite element mesh of the webs.

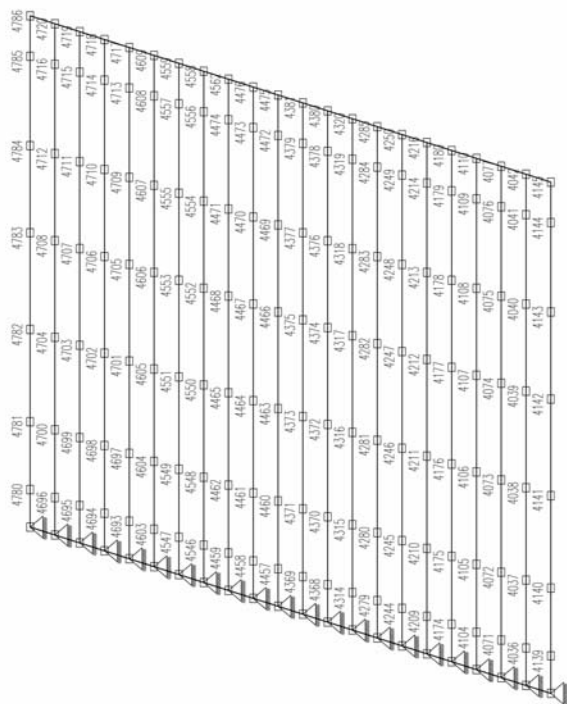


Fig. 9 FINITE ELEMENT MESH OF THE WEB .

11 Calculations and Result

Calculation and results are illustrated as follows:

11.1 One Dimensional Model:

For one dimensional model the whole box girder section is considered as one unit. The model is composed of two continuous spans each 34m. This beam is subjected to both dead and live loads. Live loads are according to AASHTO loading multiplied by 1.5 to encounter for unexpected loading. The calculations of dead and live loads are carried out as follows:

11.1.1 Shear Force due to Dead Load

- Weight of concrete per rib = 15.3KN/m²
- Weight of Asphalt per rib = 2.6KN/m² (based on 15cm thick of asphalt layer)
- Total deal load per rib = 17.92KN/m²

One intermediate diaphragms are provided at each span. Weight of each intermediate diaphragm is 3.14KN.

Fig .10 shows the distribution dead load due to own weight and asphalt layer and one concentrated dead load at each span due to diaphragm own weight.

Fig .11 also shows the shearing force for the previous dead loads.

11.1.2 Shear Force

As mentioned previously AASHTO composed of truck loading HS 20-44 or equivalent distributed load. All of these loads are multiplied by 1.5 to encounter unexpected loading. The impact factor I is equal to 27.5%.

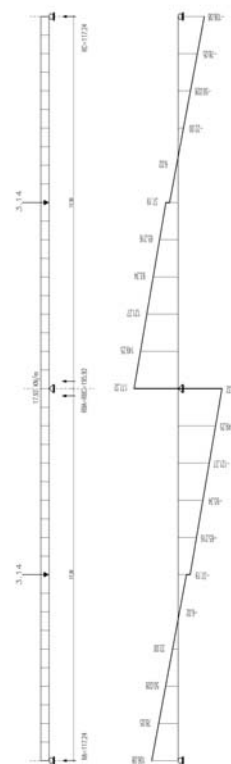


Fig: (10) SHEAR FORCE DUE TO DEAD LOAD

Fig .11 and Table 1 shows the beam divided to 10 points and the positive and negative shearing forces are calculated at each point.

Table 1 Shows the Positive and Negative Shearing Forces at Each Point Due to AASHTO Truck Loadings

Point	Maximum Positive Shearing Force KN	Maximum Negative Shearing Force KN
A		
C	±141.6	0
1		
18	±120.46	-14.73

2 17	±100.03	-19.518
3 16	±80.572	-34.22
4 15	±61.23	-53.04
5 14	±44.61	-71.45
6 13	±30.02	-91.23
7 12	±13.28	-109.86
8 11	±6.62	-127.02
9 10	_____	-142.55
B	_____	156.66

5	1.3	$(-37.77+1.67 \times 44.61)$	47.75
15	1.3	$(-37.77+1.67 \times -71.95)$	204.22
6	1.3	$(-71.91+1.67 \times 30.02)$	-28.31
14	1.3	$(-71.91+1.67 \times -91.23)$	291.54
7	1.3	$(-102.91+1.67 \times 13.25)$	104.95
13	1.3	$(-102.91+1.67 \times -109.861)$	372.28
8	1.3	$(-133.91+1.67 \times 6.62)$	159.71
12	1.3	$(-133.91+1.67 \times -127.02)$	449.84
7	1.3	$(-164.91+1.67 \times 0.00)$	214.38
11	1.3	$(-164.91+1.67 \times -142.56)$	523.88
B	1.3	$(-199.90+1.67 \times 0.00)$	259.87
	1.3	$(-199.90+1.67 \times -156.06)$	598.68

The ultimate shear force due to live loads is as shown in Fig (12) While the ultimate shearing force due to dead and life loads is as shown in Fig.13. These values are based on the following combination:-

1.3(Dead load+ 1.67 × Live Load).

Table 2 shows ultimate shearing force due to this combine of loading.

Table 2 Shearing Force Due to 1.3 (DL + 1.67 LL)

Station	Total	Ultimate Share	Nu Km/m
A	1.3	$(117.24+1.67 \times 141.60)$	459.82
C	1.3	$(117.24+1.67 \times -14.73)$	120.43
1	1.3	$(86.24+1.67 \times 120.46)$	373.63
19	1.3	$(86.24+1.67 \times -14.73)$	80.13
2	1.3	$(55.24+1.67 \times 100.03)$	288.98
18	1.3	$(55.24+1.67 \times -19.518)$	29.44
3	1.3	$(24.24+1.67 \times 80.572)$	206.43
17	1.3	$(24.24+1.67 \times -34.22)$	42.78
4	1.3	$(-6.77+1.67 \times 61.23)$	124.13
16	1.3	$(-6.77+1.67 \times -53.04)$	123.95



Fig: (11) TWO SPANS BRIDGE DIVIDED TO TEN EQUAL POINTS AND SHOWING SUPPORTS A,B AND C.

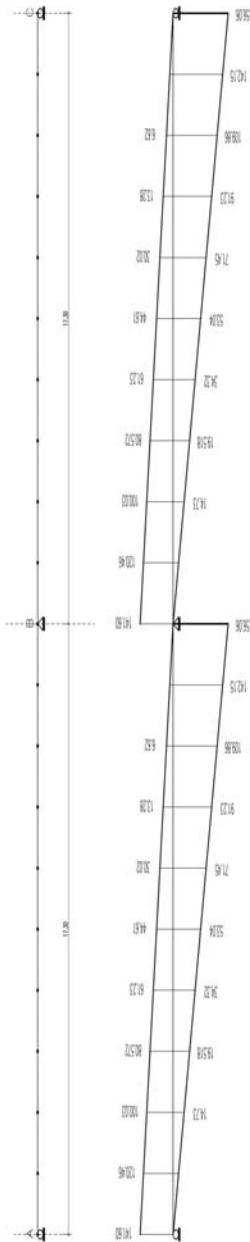


Fig: (12) SHEAR FORCE DUE TO LIVE LOAD

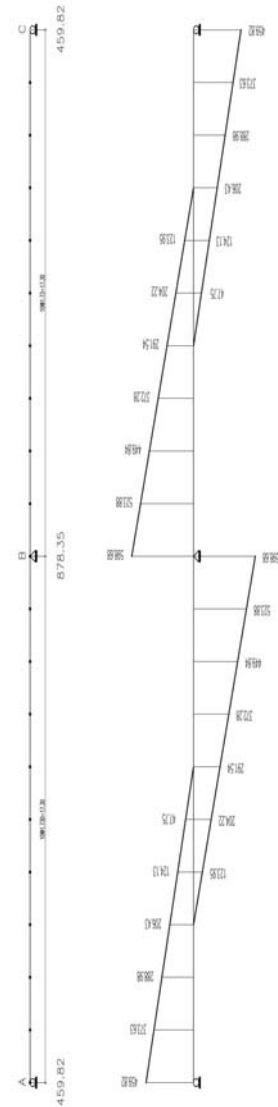


Fig: (13) ULTIMATE SHEAR FORCE DUE TO DEAD AND LIVE LOAD

11.2 Three Dimensional Finite Element Model

Figs (9) shows the finite element mesh. The shearing stresses at the top, and bottom, are studied at each finite element plate. The maximum shearing force at the exterior supports is found to be 470 KN. The max shearing force at the interior support is 617 KN.

So comparing the result obtained from the two models, it can be found that they are close enough to each other and the difference is in the arrange of 3%.

12 Conclusions

It can be concluded that designing voided slab bridges by both AASHTO specification and finite element method are acceptable and the results of the bending moments differ by almost 3% which is accepted from engineering point of view.

13 References:

- [1] Nilson, A. H and Winter, G.: **Design of Concrete Structure**, McGraw Hill Book Company, 1986.
- [2] American Association of State Highway and Transportation Officials, AASHTO: **Standard Specification for Highway Bridges**, 17th edition, Washington, 2002.
- [3] Trejo, D., and Reinschmidt, K., 2007. **Justifying Materials Selection for Reinforced Concrete Structures**. I: Sensitivity Analysis, Journal of Bridge Engineering, ASCE, Vol. 12, Issue 1, PP 31-37.
- [4] Suzuki, J., Ohba, Y., Uchikawa, Y., Hoshikawa, K., and Kimura, K., 2007. **Monitoring Temperatures on a Real Box- Girder Bridge and Energy Budget Analysis for Basic information on Bridge Cooling and Surface Freezing**. Journal of Brodge Engineering, ASCE, Volume 12, Issue 1, PP. 45-52.
- [5] Potisuk, T., and Higgins, C., 2007. **Field Testing and Analysis of CRC Deck Girder Bridges**, Journal of Bridge Engineering, ASCE, Volume 12, Issue 1, PP. 53-63.
- [6] Civjan, S., Bonczar, C., Brena, S., Dejong, J., and Crovo, D., 2007. **Integral Abutment Bridge Behavior: Parametric Analysis of a Massachusetts Bridge**, Journal of Bridge Engineering, ASCE, Volume 12, Issue 1, PP. 64-71.
- [7] Okui, Y., and Nagai, M., 2007. **Block FEM for Time - Dependent Shear - Lag Behavior in Two I-Girder Composite Bridges**, Journal of Bridge Engineering, ASCE, Volume 12, Issue 1, PP. 72-79.
- [8] Samman, M., Kennedy, J., and Sennah, K., 2007. **Impact Factors for curved continuous Composite Multiple - Box Girder Bridges**, Journal of Bridge Engineering, ASCE, Volume 12, Issue 1, PP. 80-88.
- [9] Najm, H., Patel, R., and Nassif, H., 2007. **Evaluation of Laminated circular Elastomeric Bearings**, Journal of Bridge Engineering, ASCE Volume 12, Issue 1, PP. 89-97.
- [10] Garrett, G., 2007. **Analytical Load Rating of an Open- Spandrel Arch Bridge: Case Study**, Journal of Bridge Engineering, ASCE, Volume 12, Issue 1, PP. 13-20.
- [11] Kayal, S., 2007. **Plastic Rotation of an RCC T- Beam Bridge Girder under the Combined Influence of Flexure and Torsion**, Journal of Bridge Engineering, ASCE, Volume 12, Issue 1, PP. 21-30.
- [12] Trejo, D., and Reinschmidt, K., 2007. **Justifying Materials Selection for Reinforced Concrete structures II: Economic Analysis**, Journal of Bridge Engineering, ASCE, Volume 12, Issue 1, PP. 38-44.
- [13] Guzda, M., Bhattacharya, B., and Mertz, D., 2007. **Probabilistic Characterization of Live Load Using Visual Counts and In-Service Strain Monitoring**, Journal of Bridge Engineering, ASCE, Volume 12, Issue 1, PP. 130-134.
- [14] Hon, A., Taplin, G., and Al- Mahaidi, R., 2005. **Strength of Reinforced Bridge Decks Under Compressive Membrane Action**, Structural Journal, ACI, Volume 102, Issue 3, PP. 393-401.
- [15] Taylor, S., Rankin, B., Cleland, D., and Kirkpatrick, J., 2007. **Serviceability of Bridge Deck Slabs With Arching Action**, Structural Journal, ACI, Volume 104, Issue 1, PP. 39-48.
- [16] Mankar, A., Tiwari, S., Bhargava, P., and Bhandari, N., 2006. **Load Distribution Factors for Composite Multicell Box Girder Bridges**, Advances in Bridge

Engineering, March 24-25.

[17] Dwivedi, A., Bhargava, P., and Bhandari, N., 2006. **Temperature Effects in the Design of Concrete Bridges**, Advances in Bridge Engineering, March 24-25.

[18] Menassa, C., Mabosut, M., Tarhini, K., and Frederick, G., 2007. **Influence of Skew Angle on Reinforced Concrete Slab Bridges**, Journal of Bridge Engineering, ASCE, Volume 12, Issue 2, PP. 205-214.

[19] Yehia, S., Abudayyeh, O., Nabulsi, S., and Abdelqader, I., 2007. **Detection of Common Defects in Concrete Bridge Decks Using Nondestructive Techniques**, Journal of Bridge Engineering, ASCE, Volume 12, Issue 2, PP. 215-225.

[20] Leem A., Potisuk, T., and Forrest, R., 2007. **High - Cycle Fatigue of Diagonally Cracked RC Bridge Girders: Laboratory Tests**, Journal of Bridge Engineering, ASCE, Volume 12, Issue 2, PP. 226-236.

[21] Samman, M., Kennedy, J., and Sennah, K., 2007. **Dynamic Analysis of Curved Continuous Multiple - Box Girder Bridges**, Journal of Bridge Engineering, ASCE, Volume 12, Issue 2, PP. 184-193.

[22] Zhang, H., 2007. **Determination of Allowable Differential Settlement in Bridge Approach due to Vehicle Vibrations**, Journal of Bridge Engineering, ASCE, Volume 12, Issue 2, PP. 154-163.

[23] Jaeger, L. G., and Bakht, B., "The Grillage Analogy in Bridge Analysis", **Canadian Journal of Civil Engineering**, Vol. 9. Part 2, 1982, PP. 224-235.

[24] Logan, D. L. 1986. **A First Course in the Finite Element Method**. PWS Publishers, U. S. A.

[25] Tiedman, J. Albrecht, P. and Cayes, L. 1993. Behavior of Two-Span **Continuous Bridge Under Truck Axle Loading**. Journal of Structural Engineering, 119 (4): 1234-1250.

[26] Corley, W. G. Huang, T. and Jurkovich, W.

J. 1973. **Preliminary Design and Proportioning of Reinforced Concrete Bridge Structures**. ACI Journal. 70 (5): 328-336.

[27] Research Engineers, Inc.: **STADD III/ISDS Manual**, Revision 22. April 2001. PP. 2/10-2/17.